



Research on Information Extraction of the Dongting Lake Ecological Wetland Based on Genetic Algorithm Optimized Convolutional Neural Network

Diandi Wan* and Shaohua Yin

Business School, Central South University of Forestry and Technology, Changsha, China

OPEN ACCESS

Edited by:

Yusen He,
Grinnell College, United States

Reviewed by:

Kuldeep Singh,
Govt Polytechnic Manesar, India
Sandeep Kumar Duran,
Lovely Professional University, India

*Correspondence:

Diandi Wan
WDD1593577@163.com

Specialty section:

This article was submitted to
Environmental Informatics
and Remote Sensing,
a section of the journal
Frontiers in Ecology and Evolution

Received: 15 May 2022

Accepted: 31 May 2022

Published: 28 July 2022

Citation:

Wan D and Yin S (2022) Research on Information Extraction of the Dongting Lake Ecological Wetland Based on Genetic Algorithm Optimized Convolutional Neural Network.
Front. Ecol. Evol. 10:944298.
doi: 10.3389/fevo.2022.944298

Dongting Lake is an important lake wetland in China. How to quickly and accurately obtain the basic information of the Dongting Lake ecological wetland is of great + significance for the dynamic monitoring, protection, and sustainable utilization of the wetland. Therefore, this article proposes the information extraction of the Dongting Lake ecological wetland based on genetic algorithm optimized convolutional neural network (GA-CNN), an analysis model combining genetic algorithm (GA) and convolutional neural network (CNN). Firstly, we know the environmental information of Dongting Lake, take Gaofen-1 image as the data source, and use normalized vegetation index and normalized water body index as auxiliary data to preprocess the change detection of remote sensing images to obtain high-precision fitting images. GA-CNN is constructed to efficiently extract the information of the Dongting Lake ecological wetland, and the Relu excitation function is used to improve the phenomenon of gradient disappearance and convergence fluctuation so as to reduce the operation time. Logistic regression is used for feature extraction, and finally the automatic identification and information extraction of the Dongting Lake ecological wetland are realized. The research results show that the method proposed in this article can more deeply dig the information of ground objects, express depth features, and has high accuracy and credibility.

Keywords: Dongting Lake, normalized water body, wetland information extraction, GA-CNN, normalized vegetation

INTRODUCTION

Dongting Lake is located in the middle reaches of the Yangtze River. It can protect the ecological balance, and has a great influence on the sustainable development of the Yangtze River. However, due to the long-term accumulation of silt and sand, geological and geomorphological changes, and people's interference, the Dongting Lake wetland can be said to be in ruins, and its area is getting smaller and smaller. Wetlands can effectively regulate the natural environment, and the formation of wetlands is due to the interaction between water and land, resulting in a variety of ecosystems (Zhu, 2019). At present, remote sensing technology has been widely used in wetland information extraction, resource monitoring, and other research, which is of great significance to wetland research (Jordan and Dongbo, 2019).

Wu and Daoli (2011) select TM remote sensing data of Dacang Township, Duolun County; use normalized difference acquisition index (NDVI) threshold for water body extraction the shape

characteristics of the water body, and SPOT 5 satellite image to correct the meadow components decomposed by LSMM; and extracts the wetland information after water removal by linear spectral mixing model (LSMM), so as to further extract the meadow information with high, medium, and low coverage. Sun et al. (2013) select the Nanweng River Basin in the Daxinganling forest area as the research area, and uses multi-temporal and medium-resolution environmental satellite images as data sources. Using the object-oriented method, wetland information can be extracted quickly through multi-scale segmentation, feature extraction, and decision tree construction. The effectiveness of the object-oriented method in extracting forest wetland information is systematically analyzed. In the literature (Xue and Liu, 2012), unsupervised classification results are taken as a template, the idea of zoning and grading classification is adopted, knowledge rules are obtained by analyzing the spectral information, texture information, and principal component transformation information of remote sensing images, and the method of knowledge rule correction is used to correct the ecotone of reed, *Spartina*, and *Artemisia halophila*. Experiments show that the division and hierarchical classification based on GIS rules and knowledge rules are effective methods. Wentao et al. (2020) combine the time series Sentinel-1 data with the object-oriented wetland information extraction method, and classifies Zhalong wetland using the time series C-band dual-polarization (VV, VH) Sentinel-1 data, combined with the object-oriented image analysis technology. The best time to extract Zhalong wetland information using Sentinel-1 data is May, July, and August. According to the inversion of hydrological characteristics, Yan et al. (2014) hold that the extraction methods based on geographical and ecological environment include classification methods based on hydrological geomorphology, optical remote sensing, and microwave remote sensing. Image feature extraction methods include decision tree based on radar scattering features, random forest decision tree, and aerial photo visual interpretation method. The angle method based on image information processing unit mainly includes two methods based on pixel and object classification. Sun et al. (2010) put forward that, according to the characteristics of rivers with obvious channel information, the edge extraction method based on the improved Canny operator is used to extract the river wetland information from ETM + images. The experiment shows that this method comprehensively utilizes the spectral characteristics and structural characteristics of river wetlands and achieves good results.

Traditional wetland survey methods have many problems, such as high cost, small scope, and poor timeline. Therefore, this article proposes the research on information extraction of the Dongting Lake ecological wetland based on genetic algorithm optimized convolutional neural network (GA-CNN), an analysis model combining genetic algorithm (GA) and convolutional neural network (CNN). The use of the GA-CNN model can obtain more accurate classification results of land cover types of Dongting Lake wetland, provide more accurate methods for Dongting Lake wetland information extraction, enrich research methods in the field of wetland information extraction, and provide strong support for realizing efficient and accurate

monitoring of Dongting Lake wetland and protection of the ecological environment.

GENERAL SITUATION AND DATA INTRODUCTION OF DONGTING LAKE WETLAND

An Overview of Dongting Lake

Dongting Lake is located in the northeast of Hunan Province Technology and Application, 201. The study covers 21 counties (cities, districts) in Yueyang, Changde, and Yiyang, accounting for 12.5% of the total area of Hunan province. The study area is below 50 m above sea level, with many plains and hills, and belongs to subtropical monsoon climate (Bai, 2017). The wetland vegetation in the study area is mainly composed of rice (double cropping rice and single cropping rice), reed, poplar, and *Carex* (Liu et al., 2019).

The Dongting Lake area is located in the northwest margin of the Jiangnan platform anticline, adjacent to Yangtze quasi-geosyncline in the northeast, and adjacent to the Hubei-Guizhou platform syncline in the northwest. Mesozoic movement made this area into a graben basin with the development of ancient lakes (Zhang and Liu, 2020). The landform of the Dongting Lake area is a typical alluvial-silting plain with land composite delta as the main body, which is mainly composed of muddy sand, sandy mud, and clay mud, and the ground elevation is generally between 35 and 40 m. The sediment input from Songzi, Taiping, Ouchi, and Tiaoxian and the four rivers of Hunan, Capital, Yuan, and Li, especially a large amount of sand coming through these four mouths, is the material basis for the formation of this vast plain (Pohl and van Genderen, 2016). The outer edge of Dongting Lake has 3–4 terraces, which form hills around the lake and are the transition zone between the plain of Dongting lake and the surrounding mountains. The terraces are 8–12, 20–25, 35–45, and 60–70 m higher than the lake surface, respectively. Among them, two terraces with relative elevations of 8–12 and 20–25 m are the best developed and most widely distributed (Kamusoko, 2019).

Remote Sensing Image Data

The remote sensing image data selected in this study include Landsat8 OLI and MODIS 13Q1, which are downloaded from the US Geological Survey (Ghahremani et al., 2019). The remote sensing data covering the Dongting lake wetland are shown in **Table 1**.

The acquired Landsat8 OLI data have good quality, and the cloud coverage rate is less than 5%. The software uses NDVI5.1 for radiometric calibration of data, and performs atmospheric correction through the FLAASH module. Then, based on the terrain data, the quadratic polynomial is used for geometric fine correction, and the error is less than 0.5 pixel.

The adopted data are NDVI data in MODIS 13Q1 products (Wang et al., 2020). The period is from 1 January 2021 to 19 February 2021, with 23 stages in total. The resolution is 250 m, and the projection is sinusoidal. The projection and spatial

TABLE 1 | Remote sensing data.

Data type	Rank and rank	Get date
Landsat8 OLI	123/39	All images with cloud cover<5% in 2021
	123/40	
	124/39	
	124/40	
MODIS 13Q1	H27v05	There are 23 issues from January to December 2021
	H27v06	

resolution of MODIS 13Q1 is set to be consistent with Landsat8, and are registered with Landsat8.

Other auxiliary data include field survey data, 2 m spatial resolution GF-1 (normal water period) and high-resolution images of Google Satellite Map, and phenological observation data.

Normalized vegetation index (NDVI) cannot only show the distribution of vegetation, but also reflect the growth state of vegetation, so it is widely used in the research of vegetation coverage monitoring, the extraction of vegetation distribution range, and detection of vegetation health and growth state. The calculation formula is shown in Formula (1):

$$NDVI = \frac{p_{nir} - p_{red}}{p_{nir} + p_{red}} \tag{1}$$

Normalized Difference Water Index (NDWI), a normalized water body index, which is used to extract water body information from images, has a good effect (Begg et al., 2019). The calculation formula is shown in Formula (2).

$$NDWI = \frac{p_{green} - p_{nir}}{p_{green} + p_{nir}} \tag{2}$$

where p_{green} , p_{red} , and p_{nir} represent the reflectivity of green band, red band, and near infrared (IR) band of Gaofen-1 remote sensing image, respectively.

There is a stable linear relationship between two images of the same spectral range in the same area with different phases and similar seasonal phases, so two-phase images can be used. a and b are stable ground objects in D_{dn} value, carry out correlation analysis, establish the regression equation, and put b . The radiation conditions of the image assimilate to a medium image D_{dn} . This method is often used as the preprocessing of remote sensing image change detection (Yang et al., 2020).

According to the two remote sensing images, we can select the bands with the same spectral range and carry out the relative radiation correction one by one. The regression analysis model of a single band is as follows:

$$\begin{pmatrix} Y_1^b \\ Y_2^b \\ \dots \\ Y_n^b \end{pmatrix} = a \times \begin{pmatrix} X_1^b \\ X_2^b \\ \dots \\ X_n^b \end{pmatrix} + b + \begin{pmatrix} \varepsilon_1^b \\ \varepsilon_2^b \\ \dots \\ \varepsilon_n^b \end{pmatrix} \tag{3}$$

where a, b are the coefficients representing the regression equation, and $(y^b, y_2^b, \dots, y_n^b)^T$ is the first reference image. p band

n pixels of stable figure points D_{dn} value. $(x^q, x_2^q, \dots, x_n^q)^T$ represents the first image to be returned. q band n cells of corresponding figure points with the same name. D_{dn} value, ε_1 conforms to standard normal distribution $i = 1, 2, \dots, n$.

By solving the regression coefficient using the least squares method, the formula can be obtained as follows:

$$b = \left[\sum_{i=1}^n [(x_1^q - \bar{x}^q)(y_1^p - \bar{y}^p)] \right] / \sum_{i=1}^n (x_1^q - \bar{x}^q)^2, \tag{4}$$

$$a = \bar{y}^p - \bar{b}x^q. \tag{5}$$

where \bar{y}^p denotes the substitute of the reference image number, p is the average value of the pixel values of the selected stable feature points in the band, \bar{x}^q represents the first image to be normalized, and q is the average value of pixel values of the selected stable feature points in the band (Bai, 2017).

The equation is used to correct the relative radiation of multi-temporal remote sensing images. The formula is

$$\hat{x}_{ij}^q = a \cdot x_{ij}^q + b, \tag{6}$$

where x_{ij}^q indicates the first image to be normalized q band i Hangdi j column after relative radiation correction D_{dn} value. \hat{x}_{ij}^q indicates the first image to be normalized q band i Hangdi j column pixels after relative radiation correction D_{dn} value. Then, the fitting accuracy of regression equation is judged by correlation coefficient and mean square error (Zeng and Xia, 2012).

The expression for calculating the correlation coefficient is as follows:

$$R = \frac{\sum_{i=1}^n (x_i - \bar{x})(y_i - \bar{y})}{\left[\sum_{i=1}^n (x_i - \bar{x})^2 \right]^{\frac{1}{2}} \left[\sum_{i=1}^n (y_i - \bar{y})^2 \right]^{\frac{1}{2}}}. \tag{7}$$

Among them, \bar{x} is a vector. x is the mean value, \bar{y} is a vector. y is the mean value of correlation coefficient, and R the accuracy of the regression model can be measured. If the absolute value of the correlation coefficient is between 0.8 and 1.0, it means that the matched sample pairs are highly correlated. In addition, the correlation coefficient can measure the correlation between the radiation normalized image and the original image (Le et al., 2021). Generally speaking, the normalized image should still have a high correlation with the original image.

The formula for calculating the root mean square error (RMSE) is as follows:

$$RMSE = \sqrt{\frac{1}{n} \times \left[\sum_{i=1}^n (\hat{x}_1^q - x_1^q)^2 \right]}, \tag{8}$$

where \hat{x}_1^q indicates the first image to be normalized q band's first i sample points D_{dn} the estimated value of the value, x_{ij}^q indicates the band number of the image to be normalized to i sample points of D_{dn} value. The error RMSE represents the overall accuracy of linear regression equation fit. The smaller the RMSE, the closer the radiometrically corrected image is to the reference image, and the higher the fitting accuracy (Toyoda and Yuhu, 2019).

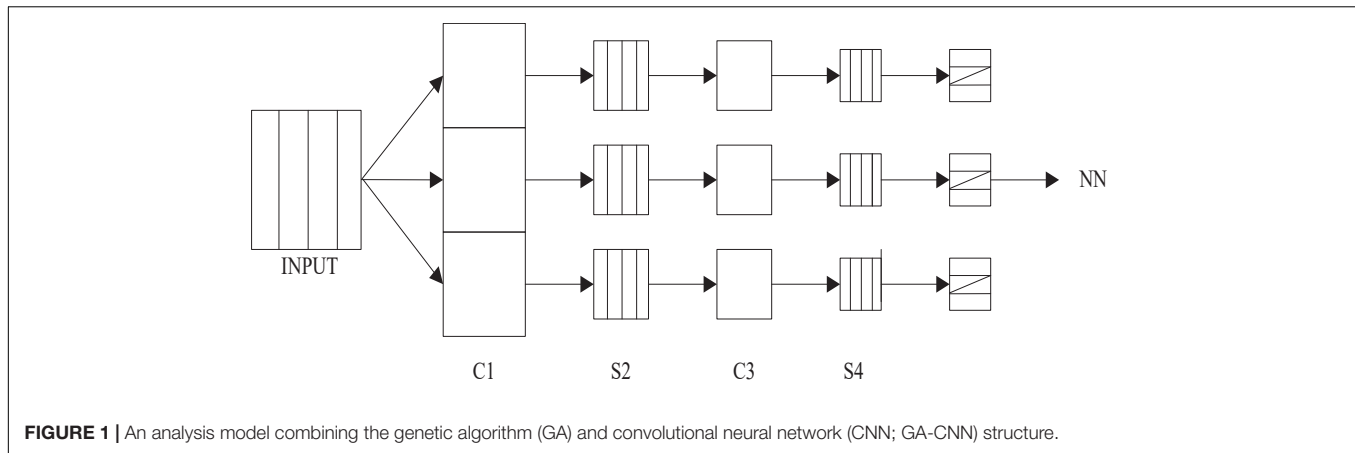


FIGURE 1 | An analysis model combining the genetic algorithm (GA) and convolutional neural network (CNN; GA-CNN) structure.

INFORMATION EXTRACTION OF ECOLOGICAL WETLAND IN DONGTING LAKE

High-resolution remote sensing images can describe the objects in detail. Compared with medium-low resolution, high-resolution images can clearly show the shape and texture of objects (Wu et al., 2020). Therefore, high-resolution remote sensing images can be widely used in the fields of surface survey and feature classification.

An analysis model that combines GA and CNN can directly input the original image, avoiding complicated image preprocessing, so it has been widely used. It is able to identify two-dimensional (2D) graphics that are invariant to translation, scaling, tilt, distortion, and other deformations. The local perception area of the image is input as the lowest level, and then it is input to other levels in turn. Each layer gets the most important features of the image through a filter. GA-CNN local weight sharing structure has certain advantages in information identification (Zhang et al., 2022). It is not necessary to select training samples according to prior knowledge, and then classify the Dongting Lake ecological wetland data after extracting category features, thus avoiding the process of manual selection and analysis of training samples.

The convolutional neural network is a multi-layer network structure, which includes input layer, convolution layer, convergence layer, full connection layer, and output layer. Each layer of the network has a 2D plane composed of multiple independent neurons. The structure of CNN is shown in **Figure 1**.

Among them, layer C represents the feature extraction layer, and layer S represents the feature mapping layer. The image is convolved by three filters, and can be biased in C1 layer to obtain three feature maps, and then three feature maps are generated in S2 layer by the excitation function. After filtration, C3 layer was obtained. As with S2 layer, each group of four pixels in the feature map is summed, weighted, and biased, and then S4 layer is obtained by the excitation function. Finally, the image pixels are rasterized, connected into vectors, are

input into the traditional neural network, and the classification results are output.

Convolution Layer

The number and size of the convolution kernels determine the number and size of the generated feature maps, and the step size determines the image acquisition density and the size of feature maps. The more convolution kernels, the stronger the network learning ability (Li et al., 2021). However, if the operation is too complicated, it will be prone to over-assembly. Therefore, when determining the number of convolution kernels, the characteristics of image data sets should be fully considered. The convolution layer reduces the number of model parameters by weight sharing, which simplifies the model. The CNN convolution process is described as follows using taking 2D images as an example.

The dimension of feature graph M and the size of the input picture. N , the scale of the convolution kernel, m and number n and sliding step size s , convolution type. The specific calculation is as follows:

1. *Number of convolution kernels*: when there are n when feature extraction convolution kernel, an input picture will be generated. n Zhang characteristic map.

2. *Convolution method*: the general convolution neural network uses zero-padding convolution or effective convolution; when the convolution kernel moves toward the image boundary, the zero-complement convolution will perform zero-complement operation outside the boundary. When the convolution is effective, convolution kernel only slides inside the picture.

3. *Step size*: The interval of each movement of the convolution kernel is called the step size. When effective convolution is used and the step size is 1, the scale size of feature graph is

$$M = \frac{N - m}{s} + 1. \quad (9)$$

Characteristic map Y is calculated as the convolution of the input image and the convolution kernel:

$$Y = X * W, \quad (10)$$

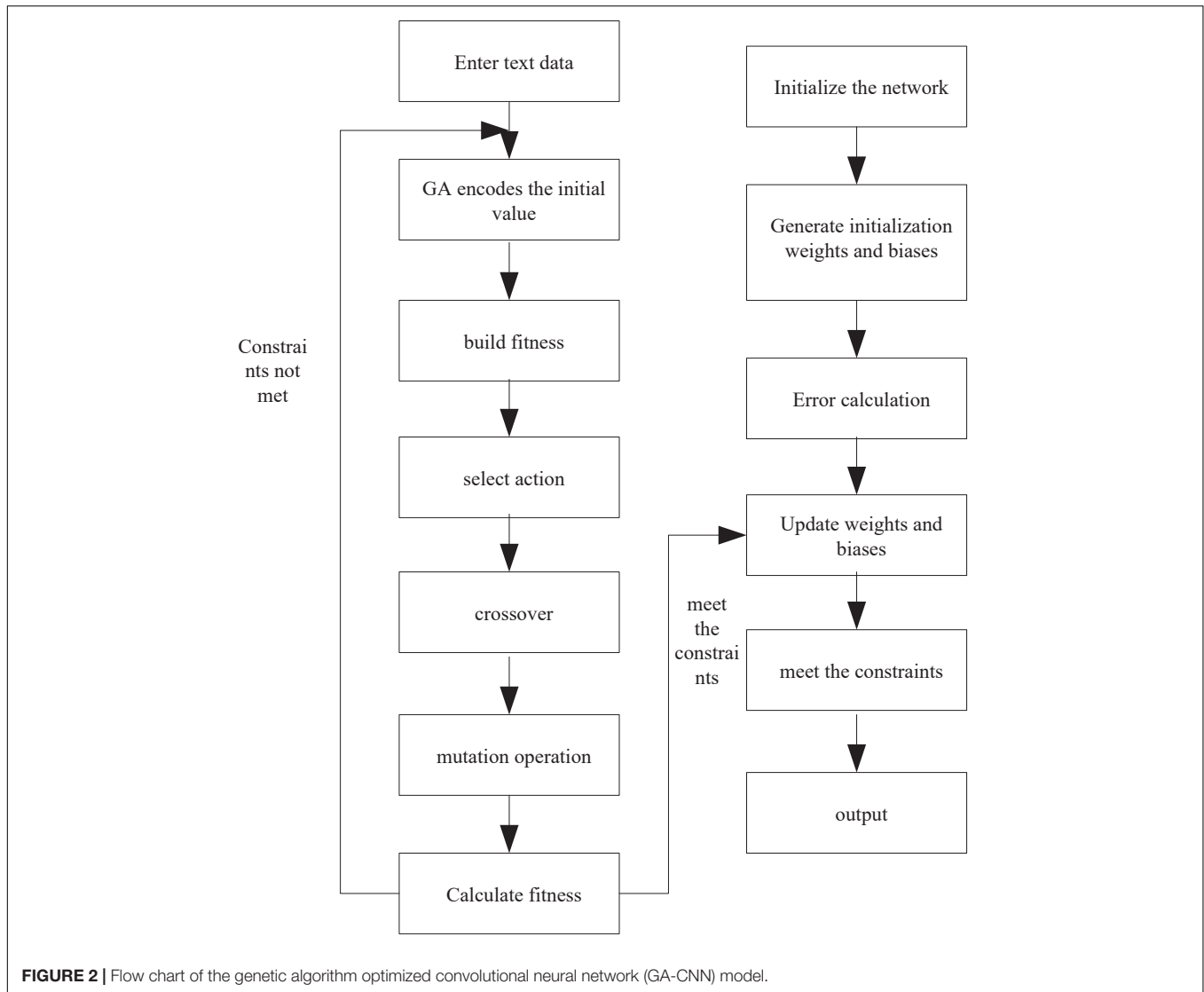


FIGURE 2 | Flow chart of the genetic algorithm optimized convolutional neural network (GA-CNN) model.

where the value of each point in the characteristic map is

$$y_{ij} = \sigma \left(\sum_{a=0}^{m-1} \sum_{b=0}^{m-1} W(a, b)X(i + a, j + b) \right). \quad (11)$$

Among (i, j) to input the 2D coordinates of the numerical points in the graph, (a, b) are the 2D coordinates of the numerical points in the convolution kernel, σ is the activation function.

Pool Layer

Pool layer is also called the feature mapping layer, and the pool process is a downsampling process. GA-CNN can directly train the image to extract features after input into the convolution layer, but the training process is complicated and the amount of calculation is large. Merging can reduce the feature dimension, improve training speed, reduce computation, and prevent overfitting. The operations include random pool, maximum pool,

TABLE 2 | Error matrix table of classification accuracy of the Dongting Lake area in 2021.

Type	Water body	Mud flat	Sedge	Reed	Woodland	Paddy field
Water body	44	3	0	0	0	0
Mud flat	12	30	1	1	0	1
Sedge	0	0	44	1	1	0
Reed	0	0	0	40	1	0
Woodland	0	0	1	5	40	1
Paddy field	6	3	1	0	0	33

average pool, etc., among which the maximum pool is the most common (Schlueter and Cowley, 2020). The input image is divided into several subregions, and the maximum value of each region is obtained as an output. Generally, after the convolution layer, the pool layer is added appropriately according to the calculation requirements.

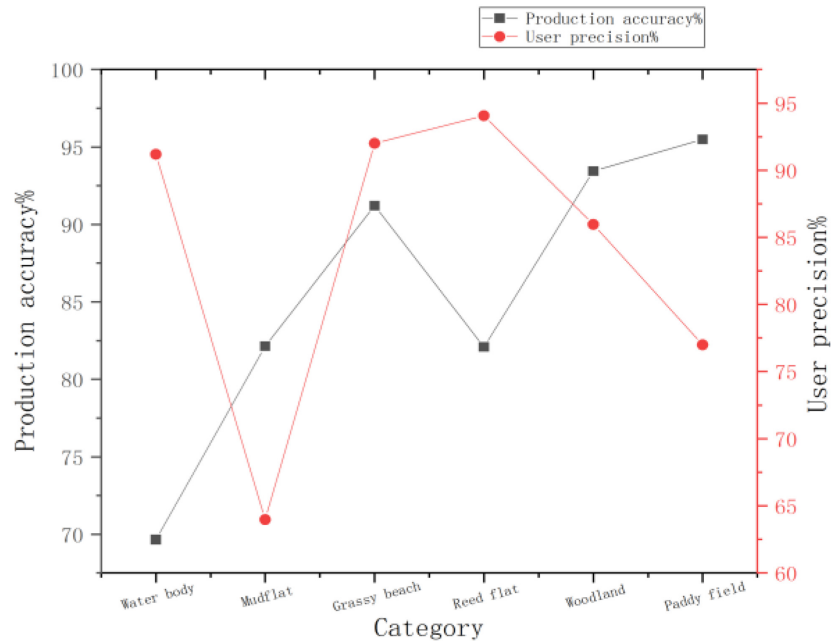


FIGURE 3 | Accuracy comparison chart.

The layers can reduce the features of each input image. Generally, the pool layer divides every two elements into 22 areas, with a maximum of four in each area. Through the calculation, the amount of data is reduced by 75%.

The pool layer and the convolution layer are combined to extract the image features twice. The network has good invariance to translation, scaling, tilt, distortion, and other deformations. The pool process is as follows:

$$x_j^l = f\left(\beta_j^l \text{down}\left(x_j^{l-1}\right)\right) + b_j^l, \quad (12)$$

where $\text{down}(\cdot)$ is the downsampling function, β^l represents multiplier parameters, and b_j^l represents an offset parameter.

Full Connection Layer

The connected layer is a special structure in CNNs, which has the function of “classifier.” (Zheng et al., 2011). After the convolution layer and the pool layer, several completely connected layers are connected, and the high-dimensional feature distribution is transformed into low-dimensional sample markers, and the learned distribution features are mapped to the sample marker space to better integrate local information and obtain abstract feature expression. All nodes in the whole connection layer are connected with each node in the previous layer, so there are more parameters in the whole connection layer. To improve the training performance of the network, accelerate the convergence speed, and prevent the gradient from disappearing, the Relu excitation function is selected in the full connection layer. Finally, the comprehensive feature information is input into the classifier for classification, and the feature extraction is carried out using softmax logistic regression (Zeng, 2019).

In practice, the convolution layer can also replace the full connection layer. Generally, the convolution kernel of 11 is used for the fully connected layer whose convolution layer is fully connected, and the fully connected layer whose convolution layer is the convolution layer that can be used in $h \times w$ convolution kernel, where h indicates the height of the convolution result obtained by the previous layer and w indicates the corresponding width.

An analysis model combining GA and CNN is used to build the model, which has eight layers. The input layer obtains the original image features, and a filter with sample characteristics is obtained. Through five convolution layers and three full connection layers, a deep learning model with eight layers of network structure is obtained, and the specific process is shown in Figure 2.

Genetic algorithm is used for global optimization in the whole network, so that each individual has all the weight parameters of the model. The model uses F_i to represent the first i feature map of a layer and uses the original image as the input layer. Suppose n represents the number of convolution layers, W_i representing the convolution kernel weight of the corresponding convolution layer, b_i indicates the offset of the corresponding layer, F_{i-1} to express the first $i-1$ the layer feature map is convolved, f represents a non-linear excitation function, a characteristic diagram F_i . The mathematical expression is

$$F_i = f\left(F_{i-1} \otimes W_i + b_i\right). \quad (13)$$

Previously, Sigmoid and Tanh non-linear excitation functions have been widely used in models. Relu is an unsaturated linear function. The acquisition of the activation value is relatively simple, only one threshold is used, and the complicated operation

process is eliminated. Therefore, to make the convergence speed faster in the descending stage of random gradient, the GA-CNN model uses the Relu excitation function to improve the problems of gradient disappearance and convergence fluctuation. The mathematical expression of Relu excitation function is:

$$f(x) = \max(0, x). \tag{14}$$

To reduce the operation time and prevent overfitting, a pool layer is added after the convolution layer to reduce the matrix size and the parameters of the full connection layer, and optimize the network. The data are input into the filter of the pool layer for calculation, and the GA-CNN model is maximized after the first, second, and fifth convolution layers, respectively. Assuming that subsampling is a downsampling function, then the pool layer F_i is

$$F_i = sub_{sampling}(F_{i-1}). \tag{15}$$

To prevent nodes with large data values from affecting the classification, the local response normalization layer is introduced in this model to improve the generalization ability of data feature learning and smooth the output of the current layer. In the formula, $a^i_{x,y}$ is the input. (x, y) zuodi i the result of sub-convolution and passing unit; n describes the number of feature maps in the same position; N is the total number of convolution kernels; k, α, β are super parameters, and the default value is set as

$$k = 2, n = 5, \alpha = 10^{-4}, \beta = 0.75, \tag{16}$$

$$b^i_{x,y} = a^i_{x,y} / \left(k + \alpha \sum^{\min(N-1, t+n/2)} (a^i_{x,y})^2 \right)^\beta. \tag{17}$$

In this model, dropout is used for the first time to prevent the neural network from overfitting in the full connection layer. The number of neurons in the input layer and the output layer is kept unchanged, and some neurons in each hidden layer are randomly deleted according to the defined probability. During the whole training process, some neurons will be randomly deleted again in each iteration. At last, in the output layer, softmax logistic regression is used to extract the information.

RESULTS AND ANALYSIS

In this article, ECognition 9.0 is used to segment the images of the Dongting Lake area to facilitate the extraction of wetland information. According to the field-measured verification points and random sampling points from Google earth, the accuracy of the GA-CNN classification method is judged by establishing the confusion matrix to calculate its mapping accuracy and user accuracy (Krivec and Guid, 2020). The confusion matrix, that is, error matrix, is a format used to evaluate accuracy, through which the user accuracy, drawing accuracy, and overall classification accuracy are calculated.

Any sample of the classification results is chosen. The probability that the category in the result graph is the same as the actual category on the ground is the user accuracy,

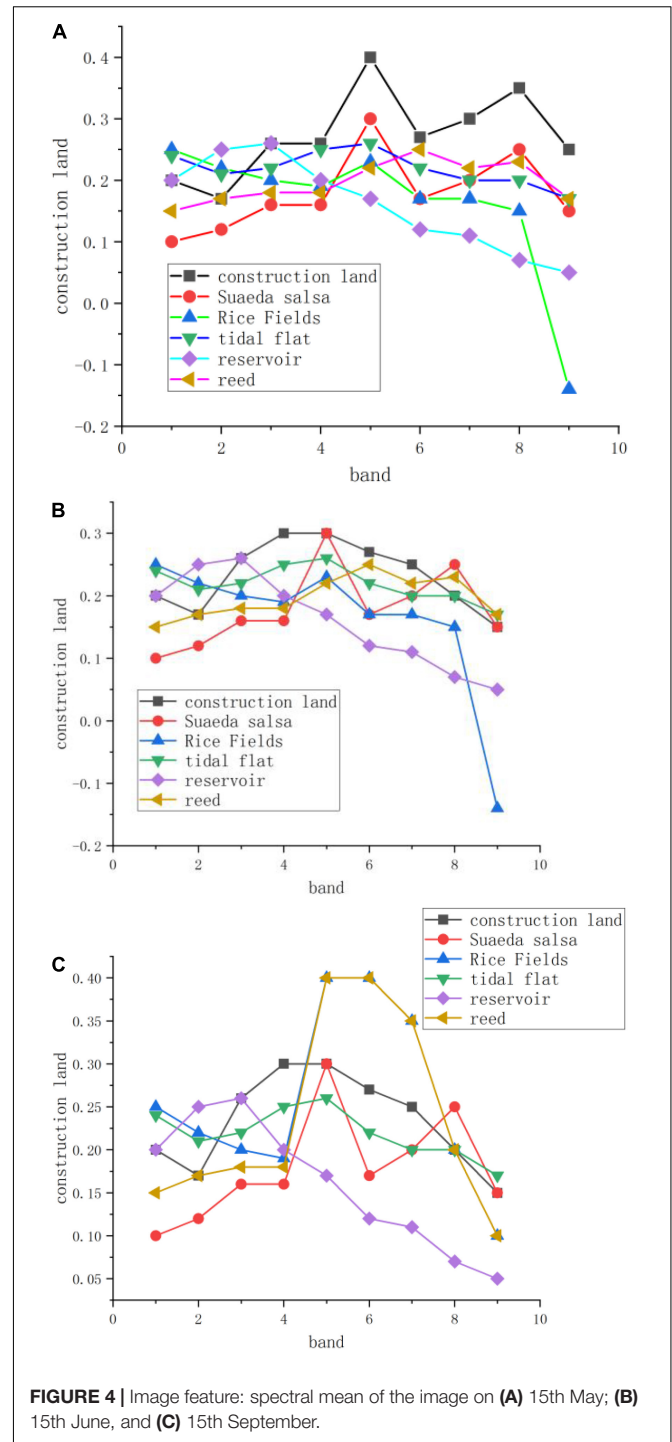


FIGURE 4 | Image feature: spectral mean of the image on (A) 15th May; (B) 15th June, and (C) 15th September.

which indicates the reliability of the classification results. Its formula is

$$p_{u_i} = \frac{p_{ii}}{p_{i+}}. \tag{18}$$

If any sample is taken, the conditional probability that the classification category in the same area is the same as the actual category in the classification result is called mapping accuracy,

and its formula is

$$p_{A_i} = \frac{p_{jj}}{p_{+j}}. \quad (19)$$

For randomly selected samples, the probability that the classification results are consistent with the actual category of the same place on the map is the overall classification accuracy, which has a probabilistic significance. Its formula is

$$p_c = \frac{\sum_{k=1}^n p_{kk}}{p}. \quad (20)$$

The Kappa coefficient, as a calculation method of classification accuracy, takes into account both user accuracy and drawing accuracy, and its expression is as follows:

$$Kappa = \frac{N \sum_{k=1}^n p_{kk} - \sum_{k=1}^n (p_{k+} p_{+k})}{N^2 - \sum_{k=1}^n (p_{k+} p_{+k})}. \quad (21)$$

ENVI software is used to evaluate the accuracy of the knowledge-based image of the study area in 2021 (He and Kusiak, 2017; Wu and Zhang, 2018; Cui et al., 2021; Li et al., 2021, 2022; Zhou et al., 2021; Li, 2022a,b). Based on the field experiment and visual interpretation, 50 sample points were selected from the original image for precision inspection. The precision error matrix and kappa coefficient are shown in **Table 2**.

As can be seen from **Figure 3**, its overall accuracy is 80.29%, and the classification accuracy is relatively higher than that of the traditional method, which proves that the data accuracy based on this method can meet the needs of practical work. Rivers, beaches and lakes, and wetlands are mixed; at the same time, paddy fields are mixed with lakes and wetlands. The most serious mixing phenomenon is mudflats. Of the 50 selected verification sites, 13 were wrongly classified as lakes and wetlands, and the lakes and wetlands were also misclassified as mudflats. The reason is that the hydrology of the Dongting Lake wetland changes greatly. Mudflat is generally the bottom of the water just above the water surface, with high water content, resulting in the mixing of water and mudflat. Paddy soil is wet, which leads to some misclassification. At the same time, paddy fields are widely distributed and crop rotation exists. Under the uniform threshold of the whole scene, it is difficult to avoid misclassification.

Because the growth difference of ground objects in different time images causes the change of spectral curve characteristics, the spectral characteristics of the same ground object in different time images often have significant differences. Therefore, a series of different time-phase data can better reflect the features of ground objects. The phenological rhythm of growth and development of wetland crops in the nature reserve is different, and the brightness values in the images are obviously different. The wetland growth process has an obvious growth rhythm, including germination, growth, flowering, fruiting, and withering. The obvious growth period of these crops is mainly from spring in April and May to autumn in August and September. Therefore, according to the phenological law of wetland features, such as reeds, the Landsat8/OLI image data in May, June, and September 2021, were selected.

At the same time, comprehensive use of these time image data to extract wetland information and better use of GA-CNN method are proposed in this article to extract feature information, so as to achieve more ideal wetland reserve classification and extraction results, and significantly improve its accuracy.

Ground verification points are randomly obtained by using the measured verification point data and Google earth images, and the accuracy is calculated by establishing the confusion matrix. In the image, the spectral curves of different crops are shown in **Figure 4**.

From the spectral features in **Figure 4**, it can be seen that the different images contain different information, and the image space used changes greatly from spring to autumn. Therefore, the image data of May, June, and September 2021 are selected for research. In the image of 15th May, the reeds in the study area are in the initial growth state, which is obviously different from other crops. In the image of 15th June, reeds grow vigorously in the study area, and the growth time between crops is different, so it is easier to distinguish crops than in May. In the image of 15th September, reed and rice in the study area grow well, and their spectral values are similar, so it is difficult to distinguish.

Image data sets with multiple different phases cover the features of different phases of the same kind of ground objects, which can more comprehensively show the features of a ground object with richer spectral features and other information in different periods. Compared with the ground features in single time image data, this feature is more detailed and comprehensive. This feature is fully utilized in the classification method to construct rule sets based on multi-temporal data.

The results show that, compared with traditional classification methods, the proposed method has high practicability in wetland classification and information extraction, which cannot only improve the classification accuracy but also reduce the time spent on data processing.

CONCLUSION

In Dongting Lake, an area affected by human factors for a long time, the certain auxiliary information is a necessary means to accurately extract wetland information in the Dongting Lake area. The proposed method takes into account the optimization performance of GA and the feature extraction ability of CNN, and can effectively screen out different kinds of ground objects with similar spectral properties. It has high accuracy in extracting ecological wetland information of Dongting Lake from remote sensing images. The accuracy of traditional methods is only 67.79%, and the kappa coefficient is 40. Compared with traditional methods, the overall accuracy of this method improves by 12.05%. The overall kappa coefficient increases by 0.1407, especially for wetland types, such as reed beach, mudflat, and paddy field. The accuracy of producers and the accuracy of users are greatly improved, and it has better generalization performance compared to traditional methods.

DATA AVAILABILITY STATEMENT

The raw data supporting the conclusions of this article will be made available by the authors, without undue reservation.

REFERENCES

- Bai, J. (2017). Wetland biogeochemistry and ecological risk assessment. *Phys. Chem. Earth* 97, 1–2. doi: 10.1016/j.pce.2017.02.004
- Begg, C. T., Matthews, V. H., Miller, R. D., Hieke, T., and Bosworth, D. A. (2019). *Introduction and General. Old Testament Abstracts*. Washington, DC: The Catholic University of America Press. doi: 10.1353/ota.2019.0018
- Cui, S., Pei, X., Jiang, Y., Wang, G., Fan, X., Yang, Q., et al. (2021). Liquefaction within a bedding fault: Understanding the initiation and movement of the Daguangbao landslide triggered by the 2008 Wenchuan Earthquake. *Eng. Geol.* 295:106455. doi: 10.1016/j.enggeo.2021.106455
- Ghahremani, M., Liu, Y., Yuen, P., and Behera, A. (2019). Remote sensing image fusion via compressive sensing. *ISPRS J. Photogramm. Remote Sens.* 152, 34–48. doi: 10.1016/j.isprsjprs.2019.04.001
- He, Y., and Kusiak, A. (2017). Performance assessment of wind turbines: data-derived quantitative metrics. *IEEE Trans. Sustain. Energy* 9, 65–73. doi: 10.1109/TSTE.2017.2715061
- Jordan, N., and Dongbo, F. (2019). Discussion on wetland ecological restoration in west dongting lake nature reserve. *Sichuan For. Surv. Des.* 25–31.
- Kamusoko, C. (2019). *Remote Sensing Image Classification in R*. Berlin: Springer Singapore. doi: 10.1007/978-981-13-8012-9
- Krivec, J., and Guid, M. (2020). The influence of context on information processing. *Cogn. Process.* 21, 167–184. doi: 10.1007/s10339-020-00958-8
- Le, S., Wu, Y., Guo, Y., and Vecchio, C. D. (2021). Game Theoretic Approach for a service function chain routing in NFV with coupled constraints. *IEEE Trans. Circuits Syst. II* 68, 3557–3561. doi: 10.1109/TCSII.2021.3070025
- Li, H. (2022a). Short-term wind power prediction via spatial temporal analysis and deep residual networks. *Front. Energy Res.* 10:920407. doi: 10.3389/fenrg.2022.920407
- Li, H. (2022b). SCADA data based wind power interval prediction using LUBE-based deep residual networks. *Front. Energy Res.* 10:920837. doi: 10.3389/fenrg.2022.920837
- Li, H., Deng, J., Yuan, S., Feng, P., and Arachchige, D. (2021). Monitoring and identifying wind turbine generator bearing faults using deep belief network and EWMA Control Charts. *Front. Energy Res.* 9:799039. doi: 10.3389/fenrg.2021.799039
- Li, H., He, Y., Xu, Q., Deng, J., Li, W., and Wei, Y. (2022). Detection and segmentation of loess landslides via satellite images: a two-phase framework. *Landslides* 19, 673–686. doi: 10.1007/s10346-021-01789-0
- Liu, Y., Yang, S., Jiang, C. R., and Deng, B. (2019). The impact of dongting lake shrinkage on the flood in the lake. *Adv. Water Sci.* 31–41.
- Pohl, C., and van Genderen, J. (2016). *Remote Sensing Image Fusion*. Boca Raton, FL: CRC Press. doi: 10.1201/9781315370101
- Schlueter, L., and Cowley, A. (2020). Review of techniques for In-Situ oxygen extraction on the moon. *Planet. Space Sci.* 181:104753. doi: 10.1016/j.pss.2019.104753
- Sun, J.-J., Ma, D.-X., Ren, C., Wang, Z.-M., and Mao, D.-H. (2013). Study on the method of wetland information extraction in nanweng river basin based on multi-temporal environmental satellite data. *Wetl. Sci.* 63–70.
- Sun, Y., Chen, D., and Qiu, Y. (2010). Research on remote sensing information extraction method of river wetlands. *Land Resour. Remote Sens.* 22–25.
- Toyoda, M., and Yuhu, W. (2019). Mayer-Type optimal control of probabilistic boolean control network with uncertain selection probabilities. *IEEE Trans. Cybern.* 51, 3079–3092. doi: 10.1109/TCYB.2019.2954849
- Wang, Y., He, Y., Yin, S., Long, H., and Li, S. (2020). Research on extraction of zinc from spent pickling solution using Aliquat 336. *Hydrometallurgy* 193:105322. doi: 10.1016/j.hydromet.2020.105322
- Wentao, C., Huan, C., and Weigang, C. (2020). Combining time series Sentinel-1 data with object-oriented wetland information extraction method. *Beijing Surv. Mapp.* 365–370.
- Wu, S., and Daoli, P. (2011). Research on wetland information extraction technology in farming-pastoral ecotone-taking Dacang Township of Duolun County as an example. *Remote Sens. Land and Resour.* 23, 130–134.
- Wu, Y., Guo, Y., and Toyoda, M. (2020). policy iteration approach to the infinite horizon average optimal control of probabilistic boolean networks. *IEEE Trans. Neural Netw. Learn. Syst.* 32, 2910–2924. doi: 10.1109/TNNLS.2020.3008960
- Wu, Y., and Zhang, Y. (2018). Evaluation of ecological economy benefit of coastal wetland of Yencheng. *IOP Conf. Ser. Earth Environ. Sci.* 186:012019.
- Xue, X., and Liu, H. (2012). Study on the classification approaches of Yancheng coastal wetlands based on ALOS image. *Remote Sens.* 3:27.
- Yan, T. T., Bian, H. F., Liao, G. X., Sheng, L., Zhang, J., and Gao, M. (2014). Research status of remote sensing information extraction methods of forest wetland. *Land Resour. Remote Sens.* 26, 11–18. doi: 10.1007/s10661-012-2661-6
- Yang, J., Guo, Y., and Wang, X. (2020). Feature extraction of hyperspectral images based on deep boltzmann machine. *IEEE Geosci. Remote Sens. Lett.* 17, 1077–1081. doi: 10.3390/s19010204
- Zeng, G. (2019). On the confusion matrix in credit scoring and its analytical properties. *Commun. Stat. Theory Methods* 49, 2080–2093. doi: 10.1080/03610926.2019.1568485
- Zeng, Z. Z., and Xia, H. S. (2012). The analysis of urban ecological wetland. *Appl. Mech. Mater.* 178-181:300. doi: 10.4028/www.scientific.net/AMM.178-181.300
- Zhang, Y., Qian, T., and Tang, W. (2022). Buildings-to-distribution-network integration considering power transformer loading capability and distribution network reconfiguration. *Energy* 244:123104. doi: 10.1016/j.energy.2022.123104
- Zhang, Y.-J., and Liu, J.-Y. (2020). Overview of research on carbon information disclosure. *Front. Eng. Manage.* 7:47–62. doi: 10.1007/s42524-019-0089-1
- Zheng, S. X., Li, J., and Sun, Q. F. (2011). Study on feature extraction method for tooth surface based on snake model. *Adv. Mater. Res.* 31, 1995–1999. doi: 10.4028/www.scientific.net/AMR.314-316.1995
- Zhou, J., Wei, J., Yang, T., Zhang, P., Liu, F., and Chen, J. (2021). Seepage channel development in the crown pillar: Insights from induced microseismicity. *Int. J. Rock Mech. Min. Sci.* 145:104851. doi: 10.1016/j.ijrmms.2021.104851
- Zhu, Y. (2019). Evaluation of ecological service value of dongting lake wetland. *Fujian Qual. Manage.* 235–236.

DW and SY completed the whole content of the article together. Both authors contributed to the article and approved the submitted version.

AUTHOR CONTRIBUTIONS

Conflict of Interest: The authors declare that the research was conducted in the absence of any commercial or financial relationships that could be construed as a potential conflict of interest.

Publisher's Note: All claims expressed in this article are solely those of the authors and do not necessarily represent those of their affiliated organizations, or those of the publisher, the editors and the reviewers. Any product that may be evaluated in this article, or claim that may be made by its manufacturer, is not guaranteed or endorsed by the publisher.

Copyright © 2022 Wan and Yin. This is an open-access article distributed under the terms of the Creative Commons Attribution License (CC BY). The use, distribution or reproduction in other forums is permitted, provided the original author(s) and the copyright owner(s) are credited and that the original publication in this journal is cited, in accordance with accepted academic practice. No use, distribution or reproduction is permitted which does not comply with these terms.